Vacuum-ultraviolet photoelectron spectroscopy of laser-excited aligned Ca atoms in the $3p$-$3d$ resonance region

M. Wedowski,[1] K. Godehusen,[1] F. Weisbarth,[1] P. Zimmermann,[1] M. Martins,[1,*] Th. Dohrmann,[2] A. von dem Borne,[2] B. Sonntag,[2] and A. N. Grum-Grzhimailo[1,†]

[1]*Institut für Strahlungs- und Kernphysik, Technische Universität Berlin, Hardenbergstrasse 36, D-10623 Berlin, Federal Republic of Germany*

[2]*II. Institut für Experimentalphysik, Universität Hamburg, Luruper Chaussee 149, D-22761 Hamburg, Federal Republic of Germany*

(Received 6 August 1996)

In this work the autoionization of the configuration Ca $3p^5 3d4s4p$ of free calcium atoms has been investigated by the use of angle-resolved photoelectron spectroscopy. In a first step, atoms in the ground-state Ca $3p^6 4s^2\,{}^1S_0$ were laser excited and aligned to the first optically excited-state Ca $3p^6 4s4p\,{}^1P_1$. From this intermediate state, with the help of synchrotron radiation (31.5–34.5 eV), the closed $3p$ subshell was opened, leading to the population of Ca $3p^5 3d4s4p$ autoionizing states. The autoionization decay of these states to both the ground state and shakeup states of singly charged ions was investigated using two types of photoelectron spectrometers. An angle-integrating spectrometer allowed us to tentatively assign the dominating angular momenta and to measure the relative partial cross sections. Furthermore, by combination with an angle-resolving spectrometer the angle dependence of the outgoing photoelectrons in the region of 32.7–33.3 eV was completely characterized for the three main diagram lines. Completeness was achieved in the sense that for action of linearly polarized light sources maximal information was extracted.

PACS number(s): 32.80.Fb, 32.80.Dz

I. INTRODUCTION

The method of combining synchrotron and laser radiation for photoionization experiments introduced in the first half of the 1980s [1–3] proved itself to be a powerful tool supplying unique direct information on the photoionization of short-lived atomic states [4]. The method was further developed in order to study photoelectron spectra from laser-excited aligned atoms [5]. By changing the direction of laser polarization additional information on the ionization into different channels was provided. A more complete exploitation of this method was achieved by introducing an angle-resolving electron spectrometer for the measurement of the angular distribution of the photoelectrons [6,7]. The angular distribution strongly depends on the geometry of the experimental setup with respect to the polarization vectors of the radiation fields and on the dynamics of the photoionization. Applications of an angle-resolved setup in experiments with lithium [6] and sodium [8,9] demonstrated its large potential. Extension of the method to targets with more complicated structure and photoionization dynamics seemed very promising. As a step in this direction we present here results on photoionization studies from the laser-excited aligned $4s4p\,{}^1P_1$ state of calcium in the region of the $3p$-$3d$ excitations.

In the Periodic Table calcium is at a position just before the beginning of the $3d$ transition metals and the contraction of the $3d$ orbital upon core excitations leads to strong configuration interaction. The properties of the $3d$ wave function of Ca are governed by the double-well-shaped potential with a delicate balance between attractive Coulomb and repulsive centrifugal parts. This wave function is fairly sensitive to small variations of the atomic central field. Therefore, photoionization in the region of the $3p$-$3d$ transitions from excited atomic calcium may reveal new features in comparison with the case of photoionization from the ground state.

Photoionization of atomic calcium has received considerable attention. A large number of the experimental investigations have been devoted to the photoionization in the region of the $3p$ inner-shell excitations from the ground state. This region has been studied by means of photoabsorption with high energy resolution [10], photoelectron spectroscopy [11], and photoion- [12,13] and angle-resolved photoelectron spectroscopy [14]. A theoretical analysis of the odd $3p$-hole states of Ca based on extensive Hartree-Fock calculations has been performed in [10]. Photoionization from the ground state in the region of the $3p$ threshold is dominated by the strong dipole resonance $3p^5 3d\,{}^1P_1$ at 31.41 eV. Due to the large $3p$-$3d$ overlap this resonance decays mainly via $3d$-$3p$ recombination with the ejection of a valence electron leaving the ion in the ground state $3p^6 4s$ and also giving rise to many satellite lines in the photoelectron spectra [11,14]. The intensity of the fluorescence emitted from the Ca^+ $4p\,{}^2P$ state in the region of the $3p$ excitations has been measured in [15] with the polarization analysis of the fluorescence in the vicinity of the $3p$-$3d$ resonance. Recently, a coincidence measurement between the angle-resolved photoelectron and the polarization-analyzed fluorescence photon of the decaying ion has been performed [16,36] in the region of this resonance with the purpose to obtain complete information about the photoionization amplitudes.

In contrast, until recently there have been no data available on the photoionization of Ca from excited

*Permanent address: Max-Planck-Institut für Radioastronomie, Auf dem Hügel 69, D-53121 Bonn, Federal Republic of Germany.

†Permanent address: Institute of Nuclear Physics, Moscow State University, 119899 Moscow, Russian Federation.

states in the vacuum-ultraviolet (vuv) energy range. Experimental results on the photoexcitation of the $3p$ electrons from the excited Ca have been obtained in [17] by using a flashlight pumped dye laser to induce the $3p^6 4s^2\,{}^1S_0 - 3p^6 4s4p\,{}^3P_1$ ($\lambda = 657.2$ nm) intercombination transition and the vuv radiation of a ruby laser produced plasma. The photoabsorption spectrum in the region 27–47 eV showed autoionizing resonances of even parity with a dominating feature at 32.3 eV. The technique of simultaneous action of laser and synchrotron radiation was applied to Ca in [18]. In that study it was combined with the method of photoelectron spectroscopy to investigate photoionization from the $3p^6 4s4p\,{}^1P_1$ excited state of Ca. A strong broad feature with a maximum at 33.03 eV photon energy was observed in the ionization channel to the ground state $3p^6 4s$ of the ion. Later the same technique was applied in [19] where advantage was taken of the possibility to change the direction of linear polarization of the pumping laser and a tentative assignment to the total angular momenta of the resonances was proposed.

In this paper we present a considerably extended set of data with improved energy resolution and statistics on the photoionization from the laser-excited aligned $4s4p\,{}^1P_1$ state of Ca in the region of the $3p$-$3d$ transitions by synchrotron radiation (SR) emitted from the electron storage ring BESSY. The photoelectron spectra are investigated for several ionization channels: to the ionic ground state $4s$, as well as to the ionic excited states $3d$, $4p$, $5s$, $4d$, $5p$, and $4f$ with a more detailed study of the three lowest channels $4s$, $3d$, and $4p$. To obtain a more complete set of data on the photoionization of aligned target atoms we utilized combined results of measurements with the angle-resolving electron spectrometer (ES) and the angle-integrating cylindrical mirror analyzer (CMA).

The experimental setup and the procedure of measurements are described in Sec. II. The geometrical aspects of photoionization by combined use of laser and synchrotron radiation beams are very useful [20]. Changing the geometry, for example, has already been applied for the identification of resonances [6,8,19]. A similar method has been used by a number of groups for low-lying autoionizing states in experiments with two laser beams. In such a case circular polarized ionizing light is easily achieved and brings in extended possibilities of the method (for Ca, see [21]). In fact, effective application of the experimental setup with a given geometry can be achieved only in combination with a broad theoretical analysis of its possibilities to obtain meaningful information on the process with a particular target. The analysis is carried out in Sec. III. Section IV contains experimental results obtained by using the CMA and a discussion based on the above-mentioned analysis. In Sec. V we consider the results of the combined use of the ES and CMA. Some results on the anisotropy of the photoelectrons in the $4s$ channel have already been published [22], but we include them in this paper for completeness.

II. EXPERIMENTAL SETUP

The experimental setup consists of three essential parts: the laser system, the synchrotron radiation source, and the vacuum chamber for the production of the atomic beam and the detection of the photoelectrons.

The laser system is used for the pumping process Ca $4s^2\,{}^1S_0 \rightarrow 4s4p\,{}^1P_1$ ($\lambda = 422.7$ nm). It is a cw ring dye laser, pumped by an argon-ion laser (4 W multiline uv) with an output power of about 150 mW (Stilbene 3) in single-mode operation. The wavelength and the single-mode operation are monitored by a wavemeter and a spectrum analyzer. Approximately 4% of the laser radiation is used to excite Ca atoms in a reference chamber in order to lock the laser to the atomic transition by the observation of the resonance fluorescence. The laser and the synchrotron radiation beams are directed into the main vacuum chamber with the electron spectrometer. They propagate antiparallel to each other and intersect the atomic beam of Ca in the interaction region in front of the electron spectrometer. Within an experimental uncertainty of a few percent both radiation beams are considered to be ideally linearly polarized. The particle density in the interaction region is kept below 10^{11} atoms/cm^3 in order to minimize radiation trapping effects which destroy the atomic alignment. The alignment is controlled by the observation of the polarization of the resonance fluorescence. However, it should be noticed that the volume probed by the photomultiplier is not exactly defined. As a consequence we expect that an averaged value of the alignment over a relatively large volume is measured, which does not necessarily coincide with the alignment present in the reaction volume. The reaction volume is defined by the region of optimal overlap of the intensity distributions of the beams participating (laser radiation beam, synchrotron radiation beam, atomic beam) and the angle of acceptance of the electron spectrometers. The low atomic density necessitates the use of the high photon flux of a wiggler-undulator beam line at the electron storage ring BESSY in Berlin. The synchrotron radiation is monochromatized by a toroidal grating monochromator (approximately 10^{13} photons/s at 34 eV within a bandwidth of 0.1 eV). The polarization axis $\vec{E}$ of the synchrotron radiation is fixed within the horizontal plane, whereas the polarization axis $\vec{A}$ of the laser radiation can be rotated by the angle η from 0° to 360° with respect to the horizontal plane by means of a Fresnel rhomb (Fig. 1).

For the electron spectrometer two different configurations are used: (a) the 180° cylindrical mirror analyzer (angular acceptance 0.8% of 4π and energy resolution 0.8% of the pass energy), which detects electrons under the ''magic'' angle $\theta_{\mathrm{CMA}} = 54.7°$ relative to the polarization axis $\vec{E}$ of the synchrotron radiation and integrates over the azimuthal angle from $-90°$ to $+90°$ [Fig. 1(a)], and (b) the simulated hemispherical spectrometer ES (angular acceptance 0.033% of 4π and energy resolution $\Delta E/E \simeq 2\times 10^{-2}$), which can be rotated in the plane perpendicular to the photon beams by the angle θ with respect to the polarization axis $\vec{E}$ of the synchrotron radiation [Fig. 1(b)].

III. THEORETICAL BACKGROUND

The geometry of the experimental setups presented in Fig. 1 is rather complicated due to several distinctive spatial directions related to the polarized laser and SR beams and the electron spectrometers. In addition, the shape of the CMA entrance slit is not trivial. Therefore, it is important to deter-

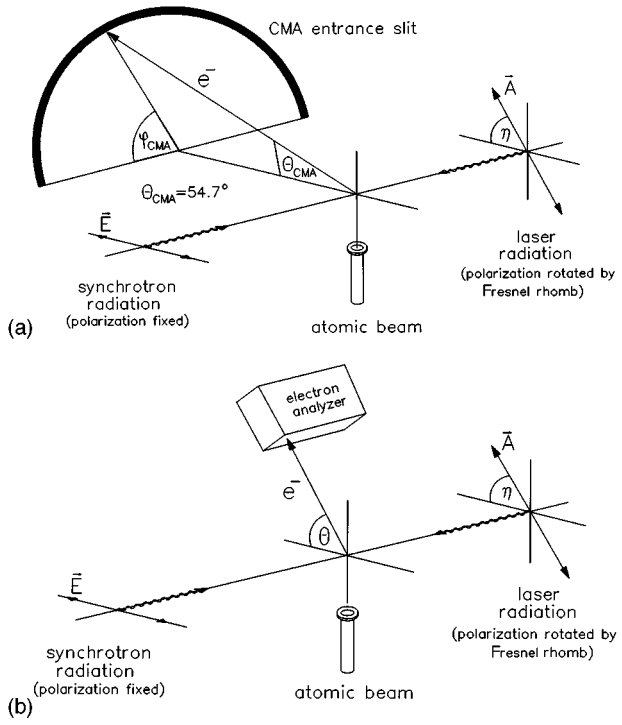

FIG. 1. Scheme of the experimental setups used for the study of the photoionization of laser-excited aligned Ca atoms (a) with the cylindrical mirror analyzer (CMA) and (b) with the rotatable electron spectrometer (ES).

mine how many independent dynamical parameters one can extract from the measurements by the above-described experimental arrangement and whether this set of parameters is complete for the particular process. Questions arise concerning the possibilities to measure the traditional quantities of the photoelectron studies: the integral cross sections from an unpolarized target $\sigma(E)$ and the correspondent coefficient of anisotropy of the photoelectrons $\beta(E)$. It would be very useful to establish the general features of the intensity variations as a function of the direction of the polarization of the laser beam and [for the setup in Fig. 1(b)] as a function of the ES position. Therefore it is necessary to clarify the possibilities of the experiments by a theoretical analysis.

A. General considerations

The theory of angular distributions of photoelectrons from polarized atoms has been the subject of many publications (for example, [23], and references therein). We use here a formalism developed in [24] in connection with the resonant photoionization by the combined use of laser and synchrotron radiation. Further considerations are necessary to analyze the potential of the present measurements. The general expression for the angular distribution can be written in the form

$$\frac{d\sigma}{d\Omega}=\frac{\sigma}{4\pi}\left(1+\sum_{k_0,k,k_\gamma}A_{k_0 0}\beta_{k_0 k k_\gamma}F_{k_0 k k_\gamma}\right), \tag{1}$$

where σ is the isotropic cross section, i.e., the photoionization cross section for unpolarized atoms. The $A_{k_0 0}$ are the normalized statistical tensors of the initial state describing the polarization of the target with the total angular momentum J_0 (these tensors are given in a frame with the z axis along the symmetry axis of the pumping process). The $F_{k_0 k k_\gamma}$ contain the geometry of the experimental setup and the polarization state of the photons. Summation in Eq. (1) is performed over all possible sets $[k_0 k k_\gamma]$ except [000]. The generalized asymmetry coefficients $\beta_{k_0 k k_\gamma}$ contain information on the dynamics of the photoionization and are expressed in terms of reduced matrix elements of the dipole operator

$$\beta_{k_0 k k_\gamma}=N^{-1}3\hat{J}_0\sum_{\gamma_f,J_f}\sum_{J,J',l,l',j,j'}(-1)^{J+J_f+k_\gamma-1/2}\hat{J}\hat{J}'\hat{j}\hat{j}'\hat{l}\hat{l}'(l0,l'0|k0)\begin{Bmatrix} j & l & \frac{1}{2}\\ l' & j' & k\end{Bmatrix}\begin{Bmatrix} j & J & J_f\\ J' & j' & k\end{Bmatrix}\begin{Bmatrix} J_0 & 1 & J\\ J_0 & 1 & J'\\ k_0 & k_\gamma & k\end{Bmatrix}$$
$$\times\langle\gamma_f J_f,lj:J\|D\|\gamma_0 J_0\rangle\langle\gamma_f J_f,l'j':J'\|D\|\gamma_0 J_0\rangle^*, \tag{2}$$

where we abbreviated $\hat{J}=\sqrt{2J+1}$. The standard notation for the Clebsch-Gordan coefficients, 6-j and 9-j symbols are used and N is the normalization factor

$$N=\sum_{\gamma_f,J_f,l,j,J}|\langle\gamma_f J_f,lj:J\|D\|\gamma_0 J_0\rangle|^2. \tag{3}$$

Summation is performed over the partial waves of the photoelectron with the orbital angular momentum l and the total angular momentum j and over the total angular momentum of the channel J. Summation over $\gamma_f J_f$ corresponds to experimentally unresolved final ionic states. Though in general the coefficients $\beta_{k_0 k k_\gamma}$ are independent dynamical parameters this is not the case in some particular situations. For example, when only channels with one total angular momentum J contribute to photoionization, the $\beta_{k_0 k k_\gamma}$ with equal values of k are proportional to each other as the dependence of k_0 and k_γ is factorized in the 9-j symbol in Eq. (2). A particular case of the generalized anisotropy parameter is the conventional coefficient of anisotropy of the photoelectrons from an unpolarized target

$$\beta=-\sqrt{\tfrac{10}{3}}\beta_{022}. \tag{4}$$

In our case we consider an atomic state with $J_0=1$ prepared by linear pumping and ionized by linear polarized SR. The

TABLE I. Kinematic factors for the geometries of experiments with the ES [$F_{k_0kk_\gamma}(\theta,\eta)$, see Fig. 1(a)] and with the CMA [$G_{k_0kk_\gamma}(\eta)$, see Fig. 1(b)].

k_0	k	k_γ	$F_{k_0kk_\gamma}(\theta,\eta)$	$G_{k_0kk_\gamma}(\eta)$
0	2	2	$-\frac{\sqrt{5}}{2\sqrt{6}}(1+3\cos 2\theta)$	0
2	0	2	$-\frac{\sqrt{5}}{2\sqrt{6}}(1+3\cos 2\eta)$	$-\frac{\sqrt{5}}{2\sqrt{6}}(1+3\cos 2\eta)$
2	2	0	$\frac{\sqrt{5}}{4\sqrt{3}}[1+3\cos2(\theta-\eta)]$	$\frac{\sqrt{10}}{\pi\sqrt{3}}\sin2\eta$
2	2	2	$\frac{5}{4\sqrt{21}}[-1+3\cos2(\theta-\eta)+3\cos 2\theta+3\cos 2\eta]$	$\frac{5\sqrt{2}}{\pi\sqrt{21}}\sin 2\eta$
2	4	2	$-\frac{\sqrt{15}}{32\sqrt{7}}[6+10\cos 2(\theta-\eta)+3\cos2\eta+10\cos 2\theta+35\cos2(2\theta-\eta)]$	$\frac{\sqrt{5}}{6\sqrt{21}}\left(\frac{7}{2}(1+3\cos2\eta)+\frac{10\sqrt{2}}{\pi}\sin2\eta\right)$

photoionization channels with $J=0$, 1, and 2 are open. The initial state is aligned and only terms with $k_0=0,2$ contribute to Eq. (1). Linear polarized SR gives values $k_\gamma=0,2$. From the triangle rule $\vec{k}_0+\vec{k}+\vec{k}_\gamma=\vec{0}$ it follows that $k\leqslant 4$. Furthermore, k is even as l and l' have the same parity due to parity conservation in the photoionization process, otherwise the Clebsch-Gordan coefficient in Eq. (2) turns to zero. As a result, only five generally independent dynamical coefficients do not vanish in Eq. (1): β_{022}, β_{202}, β_{220}, β_{222}, and β_{242}. Hence the maximum information one can get from the angular distributions when the laser and SR are linear polarized in the case $J_0=1$ consists of the six parameters: the five generalized anisotropy coefficients and the cross section σ. The next question is if the setup used, i.e., the geometry of the photon beams and the configuration of the electron detectors, allows one to measure all the parameters.

Concerning the particular geometries displayed in Fig. 1, the geometrical factors for experiments with the ES and CMA, $F_{k_0kk\gamma}(\theta,\eta)$ can be calculated [24] and the results are presented in Table I. The left column corresponds to measurements with the ES. The intensity of the photoelectrons is given as a function of the two angles θ and η,

$$I(\theta,\eta)=C_{\mathrm{ES}}\frac{\sigma}{4\pi}\left(1+\sum_{k_0,k,k_\gamma}A_{k_00}\beta_{k_0kk_\gamma}F_{k_0kk_\gamma}(\theta,\eta)\right). \tag{5}$$

The right column in Table I corresponds to the measurements with the CMA. In this case the intensity depends only on the angle η,

$$W(\eta)=C_{\mathrm{CMA}}\frac{\sigma}{4}\left(1+\sum_{k_0,k,k_\gamma}A_{k_00}\beta_{k_0kk_\gamma}G_{k_0kk_\gamma}(\eta)\right). \tag{6}$$

C_{ES} and C_{CMA} are coefficients corresponding to the efficiency of the particular experimental setup. Assuming ideal conditions, they should be angle independent. Furthermore, as a maximum, only five measurements by the ES at different pairs of angles $[\theta,\eta]$ are independent. This results from the number of linear independent trigonometrical combinations in the corresponding column in Table I (a constant representing σ also has to be taken into account). Using the CMA, as a maximum three measurements at different angles η give independent parameters. Therefore the separate experiments, either with the ES rotating in a plane perpendicular to the photon beams or with the CMA, are not enough to find the six parameters. In contrast, the combined ES plus CMA arrangement is complete for the investigation of the photoionization of aligned atoms with $J_0=1$ by linear polarized radiation. As an example, we write down one of the simplest possible set of equations defining all the five generalized anisotropy coefficients and the cross section σ in terms of directly measured intensities $I(\theta,\eta)$ and $W(\eta)$:

$$C_{\mathrm{CMA}}\sigma=\tfrac{4}{3}[W(0°)+2W(90°)]=2[W(m)+W(-m)], \tag{7}$$

$$\beta_{022}=-\sqrt{\tfrac{3}{10}}R_{0,m}, \tag{8}$$

$$A_{20}\beta_{220}=\sqrt{\tfrac{3}{5}}R_{m,m}, \tag{9}$$

$$A_{20}\beta_{202}=-\tfrac{1}{10}\sqrt{\tfrac{3}{10}}(2R_{0,0}-2R_{0,m}-R_{m,m}+8R_{m,0}+3R_{m,-m}), \tag{10}$$

$$A_{20}\beta_{222}=\tfrac{1}{20}\sqrt{\tfrac{3}{7}}(4R_{0,0}-4R_{0,m}-9R_{m,m}-4R_{m,0}-15R_{m,-m}), \tag{11}$$

$$A_{20}\beta_{242}=-\tfrac{3}{10}\sqrt{\tfrac{3}{35}}(2R_{0,0}-2R_{0,m}-R_{m,m}-2R_{m,0}+3R_{m,-m}). \tag{12}$$

The factor $R_{\theta,\eta}$ is defined by

$$R_{\theta,\eta}=\frac{I(\theta,\eta)}{I(m,0°)}\,\frac{3W(0°)}{W(0°)+2W(90°)}-1. \tag{13}$$

m denotes the magic angle ($m=54.7°$). Equations (7)–(13) correspond to the five pairs of angles in the ES mode of the experiment: $[\theta,\eta]=[0°,0°]$, $[0°,m]$, $[m,0°]$, $[m,m]$, $[m,-m]$, and two angles in the CMA mode: 0° and 90°. However, in general other combinations of angles are possible in order to obtain the same information. Note that according to Eq. (7) measurements at two different angles are needed in order to obtain the isotropic cross section σ. In contrast, for the 4π geometry as well as for the full circle entrance slit of the CMA one measurement at the magic angle would be sufficient. In general, in order to find the isotropic cross section σ by using linearly polarized photon beams one must move the detector out of the plane of the beams. This is the reason the CMA mode of the experiment is needed for measurements of σ. The total number of independent parameters that can be measured in the present studies is not enough to find in a model-independent way all dipole matrix elements including their relative phases even for the case of ionization into the ground $4s$ state of the ion. For example, by application of two linearly polarized photon beams it is impossible to obtain the isotropic cross sections for individual photoionization channels with different J and circular polarized ionizing light is needed for this purpose [25].

Using the combined ES and CMA measurements the anisotropy coefficient of photoelectrons β can be found. From Eqs. (4) and (8) one obtains

$$\beta=R_{0,m}. \tag{14}$$

Although an extraction of all the six parameters is possible by using Eqs. (7)–(13), however, it is not easy in practice to obtain all five generalized anisotropy coefficients because this can be achieved only by means of changing the angle θ at least once. This procedure is very sensitive to possible misalignments of the ES with respect to the interaction region. Finding the correct factor (13) is difficult because the C_{ES} in Eq. (5) in fact depends on θ and one must use an independent method of its correction, for example, to look for an isolated isotropic line in the spectra. The problem is much more serious than in experiments with two laser beams when the rotation of the ES can be simulated easily by the simultaneous rotation of the polarizations of the laser beams keeping the electron detector in a fixed position (for example, [26,27]). Another problem is that by switching from the CMA to the ES the effective alignment of the target can be changed. Since the value of the A_{20} is considered as a constant the formulas given above will need further correction. Finally, most of the coefficients $\beta_{k_0kk_\gamma}$ in Eqs. (8)–(12) include many terms that can give rise to large experimental error bars. Therefore, it is worthwhile to look for other possibilities of the experimental equipment that do not involve scanning over θ as well as to investigate in more detail the possibilities of measurements with the CMA.

B. Possibilities of experiments with the CMA

The general shape of the $W(\eta)$ after substitution of the geometrical factors $G_{k_0kk_\gamma}(\eta)$ from Table I is

$$\begin{aligned}W(\eta)&=C_{\mathrm{CMA}}\frac{\sigma}{4}[1+A_{20}a_{20}P_2^0(\cos\eta)+A_{20}a_{21}P_2^1(\cos\eta)]\\&=C_{\mathrm{CMA}}\frac{\sigma}{4}\left(1+\frac{1}{4}A_{20}a_{20}(1+3\cos2\eta)\right.\\&\quad\left.+\frac{3}{2}A_{20}a_{21}\sin2\eta\right),\end{aligned} \tag{15}$$

where

$$a_{20}=\frac{\sqrt{35}}{3\sqrt{3}}\left(\beta_{242}-\frac{3\sqrt{2}}{\sqrt{7}}\beta_{202}\right), \tag{16}$$

$$a_{21}=\frac{2}{3\pi}\left(\frac{10}{3}\right)^{1/2}\left(\beta_{220}+\frac{\sqrt{5}}{\sqrt{7}}\beta_{222}+\frac{5}{3\sqrt{7}}\beta_{242}\right), \tag{17}$$

and $P_k^q(\cos\eta)$ stands for the associated Legendre polynomial. As follows from Eq. (15) there are two other independent parameters in addition to the cross section σ: a_{20} and a_{21}, which can be expressed in terms of the CMA measurements at particular angles η,

$$\overline{a_{20}}:=A_{20}a_{20}=2\frac{W(0°)-W(90°)}{W(0°)+2W(90°)}, \tag{18}$$

$$\overline{a_{21}}:=A_{20}a_{21}=\frac{3}{2\sqrt{2}}\,\frac{W(m)-W(-m)}{W(0°)+2W(90°)}. \tag{19}$$

With the help of Eq. (7) one can express Eq. (19) in terms of the CMA measurements at three angles instead of four and also use different combinations of angles to obtain a_{20} and a_{21}.

General and simple results hold for the coefficients a_{20} and a_{21} in the case when only channels with the total angular momenta $J=0,1$ contribute to the photoionization process. From the triangle rules contained in the 9-j symbol in Eq. (2) it follows that $\beta_{242}=0$ and the combination $\beta_{220}+\sqrt{\frac{5}{7}}\beta_{222}$ gives strictly zero due to the particular values of the 9-j symbol. Therefore from Eqs. (16) and (17) $a_{20}=-\sqrt{\frac{10}{3}}\beta_{202}$ and $a_{21}=0$. A straightforward calculation from Eqs. (2) and (3) gives then

$$a_{20}=-\sqrt{2}\frac{\sigma_0-\frac{1}{2}\sigma_1}{\sigma_0+\sigma_1}, \tag{20}$$

where σ_0 and σ_1 are the isotropic cross sections for channels with $J=0$ and 1, respectively. When only one of the two channels contributes (for example, in the region of a strong resonance with the particular value of J) Eq. (15) takes the forms

$$W(\eta)=W_0[1-\sqrt{2}A_{20}P_2(\cos\eta)] \quad \text{for } J=0 \tag{21}$$

and

$$W(\eta)=W_0\left(1+\frac{1}{\sqrt{2}}A_{20}P_2(\cos\eta)\right) \quad \text{for } J=1, \tag{22}$$

where $P_2(\cos\eta)$ stands for the second Legendre polynomial and $W_0=\frac{1}{4}C_{\mathrm{CMA}}\sigma$. In the case of the ''ideal'' linear pumping, i.e., when only the magnetic substate with the projection $M_0=0$ is populated ($A_{20}=-\sqrt{2}$), Eqs. (21) and (22) give $\cos^2\eta$ and $\sin^2\eta$ angular dependences for channels with $J=0$ and 1, respectively. This feature has already been exploited in the first analysis of the photoionization from the excited and aligned $4s4p\,^1P_1$ state of Ca [19]. Channels with $J=2$ in general do not show a simple universal behavior and a more detailed dynamical investigation of the dipole matrix elements is needed. According to the above consideration the parameter a_{21} is nonzero only if the channel $J=2$ contributes to ionization. A nonzero parameter a_{21} may occur either directly due to a channel with $J=2$ or in the case of interference also by interaction between channels with $J=2$ and channels with other angular momenta. Therefore a positive or a negative sign of the $\overline{a_{20}}$ explicitly determines whether J equals 0 or 1, respectively, provided the $\overline{a_{21}}$ is zero, while a nonzero $\overline{a_{21}}$ can serve as an indication for the presence of channels with $J=2$. It follows from Eqs. (16) and (2) that a_{20} is free of interference effects between the channels with different J. Indeed, only channels with $J=2$ contribute to β_{242}, while β_{202} depends only on terms diagonal in J. As a result, measurements with the CMA and linear polarized photon beams give a good qualitative method for the detection of the total angular momenta of the photoionization channels.

C. The phase tilt method

In [22] an experimental method was introduced for the investigation of the angular distribution of photoelectrons from laser-aligned core-excited atoms. This method consists in the determination of the direction of laser polarization for extremal electron intensity at fixed detector configuration. Writing down Eqs. (5) and (15) for the case of the two experimental geometries shown in Fig. 1 in the form

$$I(\theta,\eta)=a(\theta)+b(\theta)\cos2[\eta-\delta^{\mathrm{ES}}(\theta)] \quad (\mathrm{ES}), \tag{23}$$

$$W(\eta)=a+b\,\cos2(\eta-\delta^{\mathrm{CMA}}) \quad (\mathrm{CMA}), \tag{24}$$

we find the general expressions for the phase tilts $\delta^{\mathrm{ES}}(\theta)$ and δ^{CMA}:[1]

$$\tan2\,\delta^{\mathrm{ES}}(\theta)=-\sin2\theta\,\frac{\beta_{220}+\sqrt{\frac{5}{7}}\beta_{222}-(5/4\sqrt{7})\beta_{242}(1+7\cos2\theta)}{\sqrt{2}\beta_{202}-\beta_{220}\cos2\theta-\sqrt{\frac{5}{7}}\beta_{222}(1+\cos2\theta)+(1/8\sqrt{7})\beta_{242}(3+10\cos2\theta+35\cos4\theta)}, \tag{25}$$

$$\tan2\,\delta^{\mathrm{CMA}}=\frac{2a_{21}}{a_{20}}, \tag{26}$$

where a_{20} and a_{21} are defined by Eqs. (16) and (17). The values of the phase tilts $\delta^{\mathrm{ES}}(\theta)$ and δ^{CMA} show the direction of the extremal electron intensities for measurements with the ES positioned at the angle θ and with the CMA, respectively. The phase tilts are very convenient quantities to measure as they are independent of the values of the alignment A_{20} in the pumped state, the intensity of the photoelectron flux, and rather insensitive to smaller changes of the experimental conditions between different runs. Therefore, the accuracy of the measurements of the phase tilts is just limited by uncertainties in the determination of the angles. Moreover, in the case of the ES measurements there is a well established reference point for counting the phase tilt $\delta^{\mathrm{ES}}(\theta)$ as it is always zero when the ES is positioned in the direction of the polarization of the SR [$\theta=0$ in Eq. (25)]. By the use of Eqs. (8)–(13), or Eq. (18) and (19), the phase tilts can also be expressed in terms of the intensities, for example,

$$\tan2\,\delta^{\mathrm{CMA}}=\frac{3}{2\sqrt{2}}\,\frac{W(m)-W(-m)}{W(0°)-W(90°)}. \tag{27}$$

Although the phase tilts (25) and (26) are rather complicated functions of the generalized anisotropy parameters $\beta_{k_0kk_\gamma}$ and hence the dipole matrix elements, they can be very useful. As follows from the preceding subsection, neglecting the photoionization channels with $J=2$ leads to $\tan2\,\delta^{\mathrm{CMA}}=0$ and $\tan2\,\delta^{\mathrm{ES}}(\theta)=0$. It has been shown in [22] how phase tilts can be used for accurate and independent measurements of the anisotropy parameter β by the ES and CMA in the special case of dominating $J=2$ channel.

Measurements with a fixed detector configuration have significant experimental advantages. Therefore, it is worthwhile to consider the possibility of obtaining a complete set of six parameters by the combined use of the CMA and the ES at fixed position $\theta=\theta_0$, i.e., only by rotation of the laser polarization. From the geometrical factors (Table I) it follows that three independent parameters can be extracted from the ES measurements which, when added to the three *parameters* from the CMA measurements, give exactly the required quantity. Nevertheless, the result is negative due to the linear dependence of the corresponding geometrical factors $F_{k_0kk_\gamma}(\theta_0,\eta)$ and $G_{k_0kk_\gamma}(\eta)$. Measurements with rotatable ES at fixed $\eta=\eta_0$ in combination with the CMA results would give the complete set of parameters.

[1]Note that our definition of the phase tilt differs from the definition of the phase shift introduced in [24] by the factor -2 for more straightforward connection with experimentally measured angular distributions.

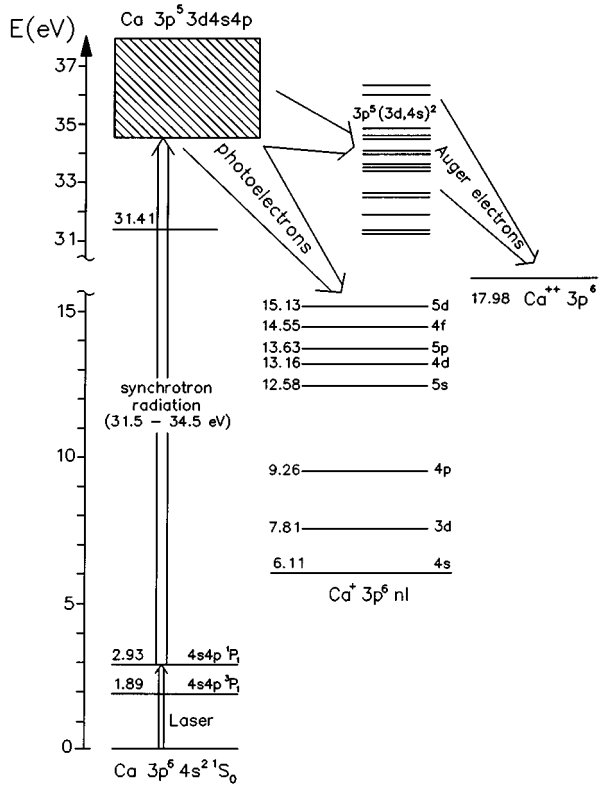

FIG. 2. Energy-level diagram of Ca, Ca^+, and Ca^{2+}. The energy scale refers to the ground state of neutral calcium. Energy levels are taken from [10,11,28,29]. Different ionization mechanisms are indicated in the figure.

IV. RESULTS OF THE CMA MEASUREMENTS

A scheme of levels related to the process under investigation is shown in Fig. 2. The position of the strong dipole resonance $3p^5 3d4s^2\,{}^1P_1$ at 31.41 eV, which can be excited from the ground state, is also marked. In the experiments we scanned the energy of the SR beam within the range 31.5–34.5 eV. Measurements with the ES were performed within the range 32.7–33.3 eV, which corresponded to the most prominent resonance feature for ionization into the $4s$ channel. The spectrometer resolution of approximately 0.2 eV in the CMA mode and 0.5 eV in the ES mode was not enough to resolve ionization into different fine structure levels of the residual ion in the excited states. In Table II the possible outgoing partial waves for the different final ionic states and total angular momenta J are summarized.

Figure 3 shows the photoelectron spectra of calcium at the photon energy of 32.9 eV, as detected by the CMA. Measurements in laser-on and laser-off modes are presented as well as the difference spectrum that corresponds to the photoelectron spectrum from the isotropic excited $4s4p\,{}^1P_1$ state. According to Eq. (7) the spectra have been obtained by combining measurements at two different angles of the laser polarization η: either 0° and 90°, or m and $-m$. Both combinations of angles gave similar results and the final spectra were taken as the average. Note that the excited-state spectra taken at different angles η, from which the spectra in Fig. 3 are determined, look quite different. The variation with the angle η is illustrated in Fig. 4.

Unfortunately, the $4p$ line from the excited state partly overlaps with the $4s$ line from the ground state, as seen from Fig. 3(a). Therefore it is difficult to isolate accurately the ionization into the $4p$ channel when the main ionization channel from the ground state shows large cross section with resonance structures. In particular, we did not investigate the range of the photon energies below 31.5 eV when the photoelectrons from the decay of the strong resonance at 31.41 eV into its main $4s$ channel disturb the photoelectron spectrum of the laser-excited atoms in the $4p$ channel.

Both spectra, from the ground and from the excited state [Figs. 3(b) and 3(c)], show many satellite lines originating from ionization with excitation. The intensity ratios of different photoelectron lines produced from the ground state at the energy 32.9 eV are very close to those observed in [11] at the same energy. Strong lines in Fig. 3(c) at energies below 17.5 eV originate from the Auger decay of the core-excited Ca^+ states $3p^5 nln'l'$ and indicate that these states are populated with high probability via the decay of the Ca autoionizing states by the ejection of low-energy electrons (Fig. 2). A very similar production mechanism for the double-charged Ca ions has been found for photoionization from the ground state at the excitation energies above the $3p^5 3d4s$ and $3p^5 4s^2$ thresholds [12,13].

We will concentrate now on the constant ionic state (CIS)

TABLE II. Allowed channels with total angular momentum J for photoionization from the excited Ca state: $Ca(4s4p\,{}^1P_1)+\gamma \rightarrow Ca^+(nl\,{}^2L_{J_f})+\varepsilon l_j$. Square brackets indicate channels that are forbidden for ionization provided the LS-coupling scheme is valid.

J	$nl(^2L_{J_f})$	εl_j
0	$4s\ (^2S_{1/2})$	$\varepsilon s_{1/2}$
	$4p\ (^2P_{1/2})$	$\varepsilon p_{1/2}$
	$(^2P_{3/2})$	$\varepsilon p_{3/2}$
	$3d\ (^2D_{3/2})$	$\varepsilon d_{3/2}$
	$(^2D_{5/2})$	$\varepsilon d_{5/2}$
1	$4s\ (^2S_{1/2})$	$[\varepsilon s_{1/2}]$
		$[\varepsilon d_{3/2}]$
	$4p\ (^2P_{1/2})$	$\varepsilon p_{1/2},\ \varepsilon p_{3/2}$
	$(^2P_{3/2})$	$\varepsilon p_{1/2},\ \varepsilon p_{3/2}$
		$[\varepsilon f_{5/2}]$
	$3d\ (^2D_{3/2})$	$[\varepsilon s_{1/2}]$
		$\varepsilon d_{3/2},\ \varepsilon d_{5/2}$
	$(^2D_{5/2})$	$\varepsilon d_{3/2},\ \varepsilon d_{5/2}$
		$[\varepsilon g_{7/2}]$
2	$4s\ (^2S_{1/2})$	$\varepsilon d_{3/2},\ \varepsilon d_{5/2}$
	$4p\ (^2P_{1/2})$	$\varepsilon p_{3/2}$
		$\varepsilon f_{5/2}$
	$(^2P_{3/2})$	$\varepsilon p_{1/2},\ \varepsilon p_{3/2}$
		$\varepsilon f_{5/2},\ \varepsilon f_{7/2}$
	$3d\ (^2D_{3/2})$	$\varepsilon s_{1/2}$
		$\varepsilon d_{3/2},\ \varepsilon d_{5/2}$
		$\varepsilon g_{7/2}$
	$(^2D_{5/2})$	$\varepsilon s_{1/2}$
		$\varepsilon d_{3/2},\ \varepsilon d_{5/2}$
		$\varepsilon g_{7/2},\ \varepsilon g_{9/2}$

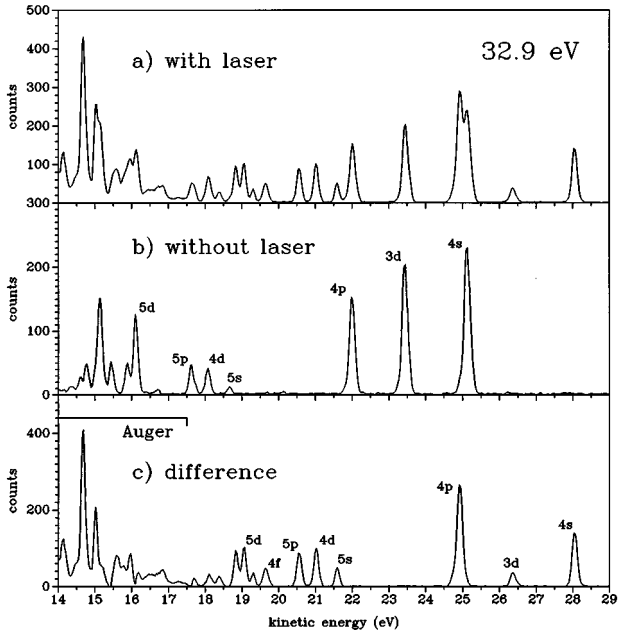

FIG. 3. Photoelectron spectra of Ca measured at 32.9 eV photon energy by the CMA: (a) laser off; (b) laser on; and (c) the difference spectrum.

spectra, i.e., on the individual cross sections of photoionization from the excited state to the first calcium ion channels $4s$, $3d$, $4p$, $5s$, $4d$, $5p$, and $4f$ as functions of the photon energy. To obtain the CIS spectra the energy window of the CMA was tuned to the photoelectron line corresponding to the particular ionic state. For the channels $4s$, $4p$, and $3d$ the measurements were performed at the angles $\eta=0°$, $90°$, m, and $-m$ of the laser polarization. By the formulas (18) and (19) the parameters $\overline{a_{20}}$, $\overline{a_{21}}$ were extracted as well as the phase tilt (26) and the cross section (7). Complete scans of η over the full circle were also performed at selected

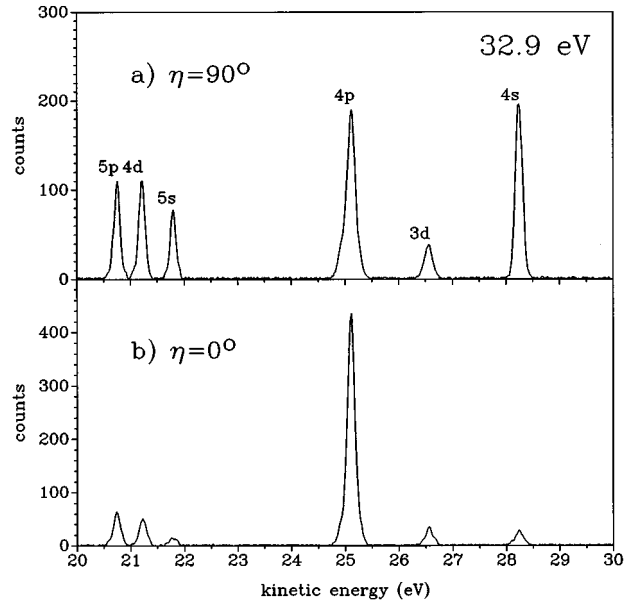

FIG. 4. Photoelectron spectra of the laser-excited Ca measured at 32.9 eV photon energy by the CMA for different directions of the laser polarization: (a) $\eta=90°$ and (b) $\eta=0°$.

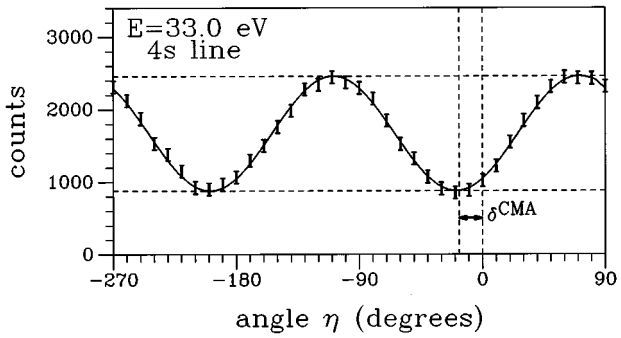

FIG. 5. Typical η scan measured at 33.0 eV photon energy by the CMA for the $4s$ ionization channel. The phase tilt δ^{CMA} is indicated.

energies. For all η scans a least-squares fit procedure using Eqs. (15) and (24) delivered results similar to those described above. A typical η scan for decay in the $4s$ ionization channel at 33.0 eV photon energy is shown in Fig. 5. The general shape of any η scan is illustrated by this example.

In photoionization from the ground state $4s^2$ the $4s$ channel is distinguished, because it can be reached by one-electron transition, while the satellites are excited from the ground state mainly by ground-state correlations. In the case of photoionization from the excited $4s4p$ state, the two channels $4s$ and $4p$ must be treated equivalently and one should speak about the two main photoelectron lines $4s$ and $4p$. Therefore, it is not surprising that the $4p$ and the $4s$ cross sections are of the same order within the energy range studied. However, the $4p$ cross sections are larger for most energies.

Figure 6 shows relative partial cross sections for the decay channels investigated. The summed cross sections for all these decay channels are shown in Fig. 6(a), the main decay channels $4s$ and $4p$ are shown in Fig. 6(b), while the satellite decay channels are depicted in Figs. 6(c)–6(e). There are dramatic differences in the coupling of the different ionization channels to the resonances. Figures 7–9 present the energy dependence of the parameters for the channels $4s$, $4p$, and $3d$ as functions of the photon energy.

In the following discussion of the individual channels with respect to the cross section, the parameters $\overline{a_{20}}$ and $\overline{a_{21}}$, and the phase tilt δ^{CMA} we use the photon energy scale, i.e., we will refer the energies to the laser-excited $4s4p\,^1P$ (2.93 eV) state.

A. Ionization into the 4s channel

Photoelectrons in the continua $\varepsilon s_{1/2}$ $(J=0,1)$, $\varepsilon d_{3/2}$ $(J=1,2)$, and $\varepsilon d_{5/2}$ $(J=2)$ are produced during the ionization into the $4s$ channel (see Table II). The CIS is dominated by the broad resonance structure with a maximum at 33.0 eV [Fig. 7(a)], which correlates well with the preceding measurements [18]. The shape of the structure shows that it is not a single resonance, but a result of several overlapping resonances. At the low-energy side of the structure a clear enhancement of the cross section is seen in the range 32.0–32.7 eV, which indicates contribution from other resonances with a more pronounced feature at 32.6 eV. Below 31.8 eV

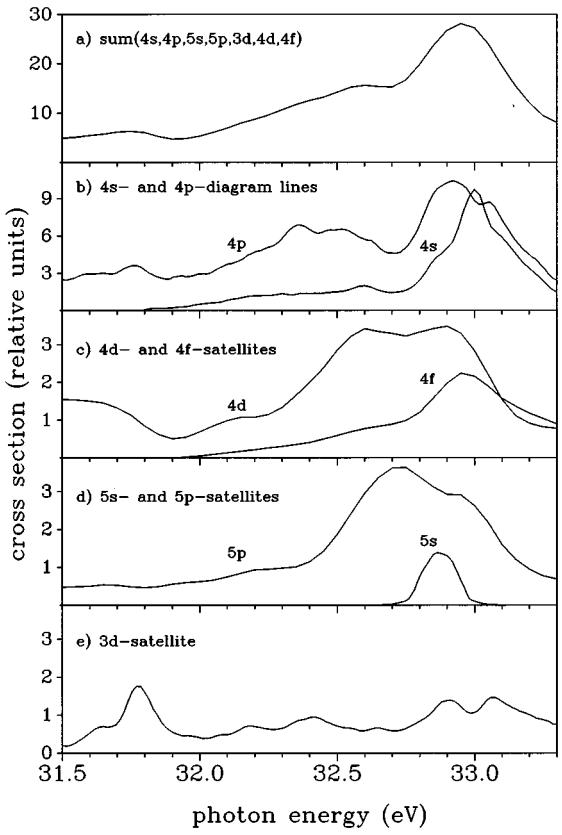

FIG. 6. Summed and partial cross sections for the photoproduction of singly charged calcium ions from the excited $4s4p\,^1P_1$ state as a function of the photon energy. The channels $4s$, $4p$, $4d$, $4f$, $5s$, $5p$, and $3d$ are taken into account. All data are presented in relative units.

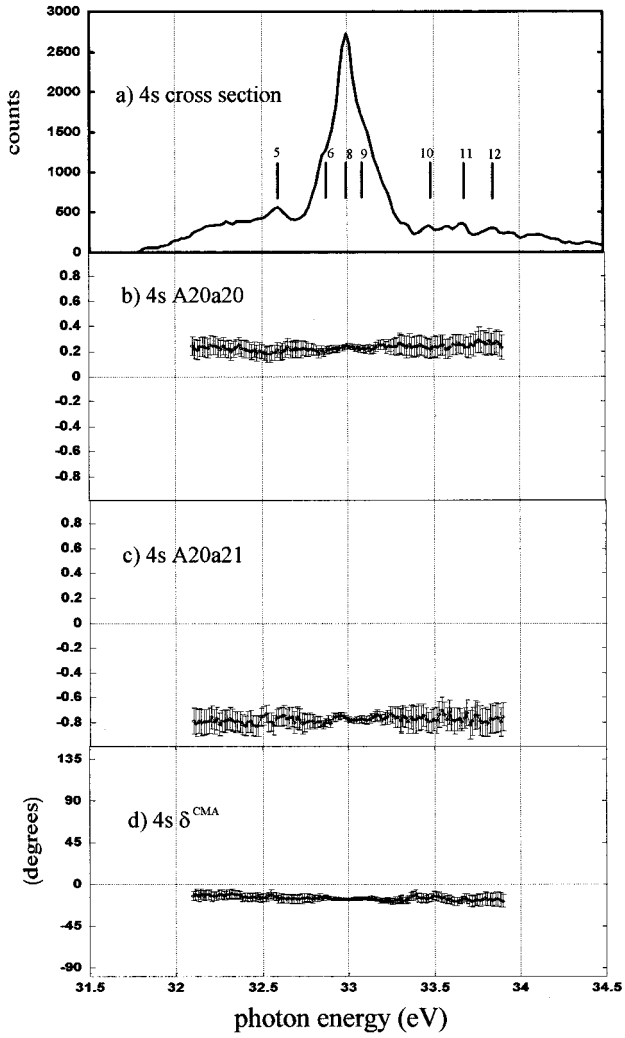

FIG. 7. The (a) cross section, parameters (b) $\overline{a_{20}}$ and (c) a_{21}, and (d) phase tilt in the $4s$ channel measured by the CMA as a function of the photon energy. The marks in (a) represent the positions of the resonance features presented in Table III.

the signal drops to zero. At the high-energy side of the main resonance one can distinguish a plateau formed out of a number of features that can hardly be separated. At photon energies within the range investigated the Ca $3p^5 4s^2\,^2P_{3/2,1/2}$ ionization thresholds 31.38 and 31.73 eV above the excited Ca $4s4p\,^1P_1$ level can be reached [10]. The other well established thresholds accessible in this range are $3p^5(3d^2\,^1S)^2P_{3/2}$ at 33.18 ± 0.03 eV and $3p^5(3d^2\,^1S)^2P_{1/2}$ at 33.46 ± 0.04 eV [10,11,30–32]. Auger lines as well as the photoionization cross section of Ca indicate other possible thresholds in the energy region under consideration [11,17,30,32] (for recent calculations of the thresholds and further references see [33]). However, there is no clear evidence that the CIS spectrum in the $4s$ channel is influenced by all these thresholds.

Figure 7(d) shows that the phase tilt is constant within the error bars ($\delta^{\mathrm{CMA}}=-15.5°\pm5.0°$) in the range of the main resonance at 33.0 eV in contrast to the rapid variation of the cross section. The constant value of the parameters $\overline{a_{20}}$ and $\overline{a_{21}}$ in Figs. 7(b) and 7(c) indicates that the broad resonance is formed primarily of contributions from channels with one value of J, namely, $J=2$, otherwise δ^{CMA} should be 0° or 90° in accordance with the discussion in Sec. III C. Therefore we identify the resonance at 33.0 eV as $3p^5 3d(^1P)4s4p$: $J=2$ with further overlapping $J=2$ resonances contributing to the main peak. Also in the region 32.1–32.7 eV the behavior of the phase tilt points to a significant contribution from channels with $J=2$, in particular, at the weaker resonance at 32.6 eV. In contrast to the cross section that is an incoherent sum of contributions from channels with different J, the phase tilt depends also on the interference between the channels $J=2$ and 1, and between $J=2$ and 0. Therefore, the phase tilt, as well as the $\overline{a_{21}}$, can be fairly sensitive to the contributions from the ionization channels with $J=0,1$. Note that in the pure LS-coupling scheme ionization from the excited state $3p^6 4s4p\,^1P_1$ into the $4s$ channel with $J=1$ is forbidden (see Table II). This can partly explain the dominant contribution from channels with $J=2$ into the $4s$ partial cross section.

Taking advantage of the fact that the main feature in the $4s$ channel results from ionization into the channels with $J=2$ one can extract in a model-independent way the value of the anisotropy parameter β from the value of the phase tilt δ^{CMA} [22]. For the $J=2$ channel Eq. (26) with the use of Eqs. (16), (17), and (2) reduces to

$$\tan 2\,\delta^{\mathrm{CMA}}=\frac{4\sqrt{2}}{3\pi}\frac{5-3f(X)}{5-f(X)}, \tag{28}$$

where

$$f(X)=1+2\frac{1+|X|^2}{1+2\sqrt{6}\ \mathrm{Re}X} \tag{29}$$

and X represents the ratio of the reduced dipole matrix elements

$$X=\frac{\langle 4s\,^2S_{1/2},\varepsilon d_{3/2}:J=2\|D\|4s4p:J_0=1\rangle}{\langle 4s\,^2S_{1/2},\varepsilon d_{5/2}:J=2\|D\|4s4p:J_0=1\rangle}. \tag{30}$$

For the case $J=2$ when only two partial waves $\varepsilon d_{3/2,5/2}$ contribute, the anisotropy coefficient β takes the form [see Eqs. (4) and (2)]

$$\beta=\frac{1}{10}\,\frac{7f(X)-5}{f(X)-1}. \tag{31}$$

Using the experimental value of δ^{CMA} one obtains from Eqs. (28) and (31) $\beta=0.84(5)$. This can be compared with the values of $\beta=1$ in the $^1D_2$ channel ($X=2/\sqrt{6}$) and $\beta=0.5$ for the $^3D_2$ channel ($X=-\sqrt{3/2}$) in the pure LS-coupling scheme. Therefore our data indicate a violation of the LS-coupling scheme for ionization into the $4s$ channel in the region of the $J=2$ resonance at 33.0 eV.

B. Ionization into the 4p and 3d channels

Results for ionization into the other main channel $4p$ and the satellite channel $3d$ are presented in Figs. 8 and 9, respectively. In addition to the cross sections the phase tilt δ^{CMA} and the parameters $\overline{a_{20}}$ and $\overline{a_{21}}$ are depicted. As a consequence of the partial overlap of the $4p$ line of the laser-excited state with the $4s$ photoelectron line of the atomic ground state the data for the $4p$ channel are less reliable. The influence is not negligible because the intensity of the ground-state signal shows prominent resonance features in the energy region investigated [inset in Fig. 8(a)]. In contrast to the $4s$ channel (Fig. 7) all parameters show complicated shapes indicating that the dominant contributions come from multiple J's. Furthermore, in most cases there is no coincidence of these features with the resonance structure of the cross section. Nevertheless, we will discuss some features in more detail and we will try to give a tentative assignment.

The resonance 2 at 31.75 eV, which is the strongest in the $3d$ channel, belongs, most probably, to a state with $J=1$. This follows from large negative value of $\overline{a_{20}}$ and negligible value of $\overline{a_{21}}$ in the $3d$ channel [Figs. 9(b) and 9(c)] and the fact that the background at resonance is relatively weak. The same feature in the $4p$ channel [Fig. 8(a)] has a strong background from channels with $J=2$. We assign tentatively the value $J=1$ also to a smaller closely spaced peak 1 at 31.65 eV and to similar features 3 at 32.20 eV and 4 at 32.40 eV. However, probably the $J=2$ background increases with energy at least up to 32.50 eV. This seems to be a common feature for all three channels $4s$, $3d$, and $4p$. Furthermore, we tentatively assign $J=2$ to the feature 5 at 32.60 eV in the $3d$ spectrum. Indeed, this feature cannot belong again to $J=1$ because of the sharp variation in $\overline{a_{20}}$ and $\overline{a_{21}}$ [Figs. 9(b) and 9(c)], whereas dominating contributions from $J=0$ are unlikely because of the nonzero values of

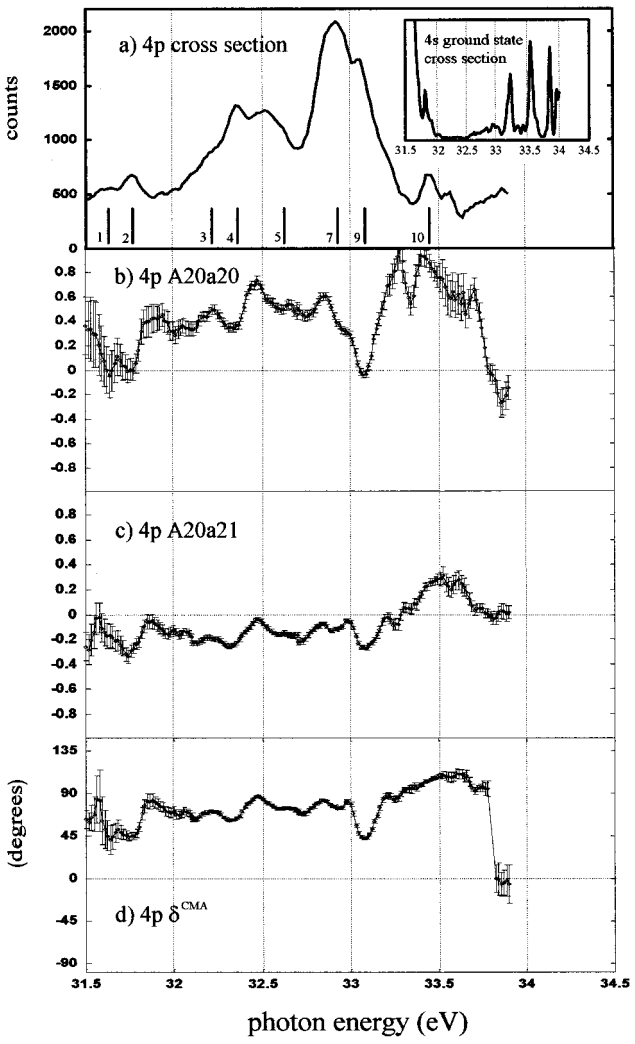

FIG. 8. The (a) cross section, parameters (b) $\overline{a_{20}}$ and (c) $\overline{a_{21}}$, and (d) phase tilt in the $4p$ channel measured by the CMA as a function of the photon energy. The marks in (a) represent the positions of the resonance features presented in Table III.

$\overline{a_{21}}$. The position at 32.60 eV is in accordance with the resonance in the $4s$ spectrum, which also showed properties corresponding to $J=2$.

A strong doublet structure 7,9 with maxima at 32.90 and 33.05 eV is seen in the cross section of both channels, though the shape of the structures differs and they likely consist of contributions from overlapping resonances. The above discussion for the $4s$ channel gives a hint that in the range 32.8–33.2 eV one can expect large contributions from the $J=2$ resonances to the spectra and that both components of the doublet are dominated by channels with $J=2$. The data for the parameters $\overline{a_{20}}$ and $\overline{a_{21}}$ in the $4p$ and $3d$ channels, however, contradict this assumption as both undergo sharp variations around 33.0 eV and one must assign different leading total angular momenta to the components. Nevertheless, contributions of $J=2$ channels to the structures is evident from the nonzero values of $\overline{a_{21}}$. A drastic drop in the $\overline{a_{20}}$ [Figs. 8(b) and 9(b)] indicates that the high-energy component 9 at 33.05 eV likely has leading channels with $J=1$. It is difficult to assign a single value of J to the low-energy component 7 at 32.90 eV. It looks as if it would in-

clude a large portion of the $J=0$ because of an increase in $\overline{a_{20}}$ at the position of the maximum, but the percentage of different J's is not the same in the $4p$ and $3d$ channels.

A feature 10 around 33.45 eV in both spectra $4p$ and $3d$ shows dominant contributions from channels with $J=2$ because of the increase in the parameter $\overline{a_{21}}$. The structure shows different shapes in the $4p$ and $3d$ spectra: there are two maxima in the $4p$ spectrum and a single maximum in the $3d$ spectrum. This may be caused by opening of the threshold $3p^5(3d^2\,{}^1S)^2P_{1/2}$ at 33.46 ± 0.04 eV.

In the following region the parameter $\overline{a_{20}}$ undergoes several very sharp jumps. Some of them can be attributed to the particular resonance features in the cross section while, for example, a rapid variation at 33.75–33.80 eV [Fig. 8(b)] does not correlate with any pronounced feature in the $4p$ spectrum. Summarizing, we give in Table III energies of the main features in the even core-excited CIS of Ca in the range of the photon energies 31.5–34.0 eV with tentative assignments of the total angular momentum of the dominating ionization channels.

C. Other channels

A limited number of measurements have been done for other photoionization channels, $5s$, $4d$, $5p$, and $4f$, which did not cover the whole energy range and were taken only for the angles $\eta=0°$ and $\eta=90°$. Relative cross sections are given in Fig. 6. The absolute values in the $4d$ and $5p$ channels are even larger than those in the $3d$ channel, while the $4f$ and $5s$ cross sections are comparable with it.

The CIS for the $5s$ channel shows a strong line 6 at 32.85 eV that coincides in the position with a structure on the low-energy slope of the main maximum in the $4s$ channel. Above we have assigned $J=2$ to this structure. We measured also the phase tilt δ^{CMA} for the line in the $5s$ channel and found it very close to those in the $4s$ channel. The signal drops to zero out of the narrow energy range 32.7–33.0 eV. It is astonishing that the main $J=2$ line of the $4s$ spectrum at 33.0 eV does not appear in the $5s$ spectrum.

For the $4d$, $5p$, and $4f$ channels the parameter $\overline{a_{20}}$ shows similar behavior in the range 32.7–33.1 eV, indicating a common mechanism of ionization into these three ionic states: from dominating $J=2$ channels at lower energies towards increasing contribution from the $J=0$ channels at higher energies. In contrast, the parameter $\overline{a_{20}}$ in the $4s$, $4p$, and $3d$ channels showed quite different behavior in this energy range. Another observation is a common sharp variation of the $\overline{a_{20}}$ starting from 33.15 eV in the channels $4p$, $3d$, $4d$, and $4f$ which indicates the threshold $3p^5(3d^2\,{}^1S)^2P_{3/2}$.

V. THE ES AND COMBINED ES PLUS CMA MEASUREMENTS

A. Generalized anisotropy parameters

The main advantage of using the combination of both setups is the possibility to make a step towards the complete experiment, i.e., to measure the complete set of generalized anisotropy parameters. We shall, however, concentrate first on the anisotropy parameter β in the $4s$ channel. As in the case of the CMA measurements presented in the preceding

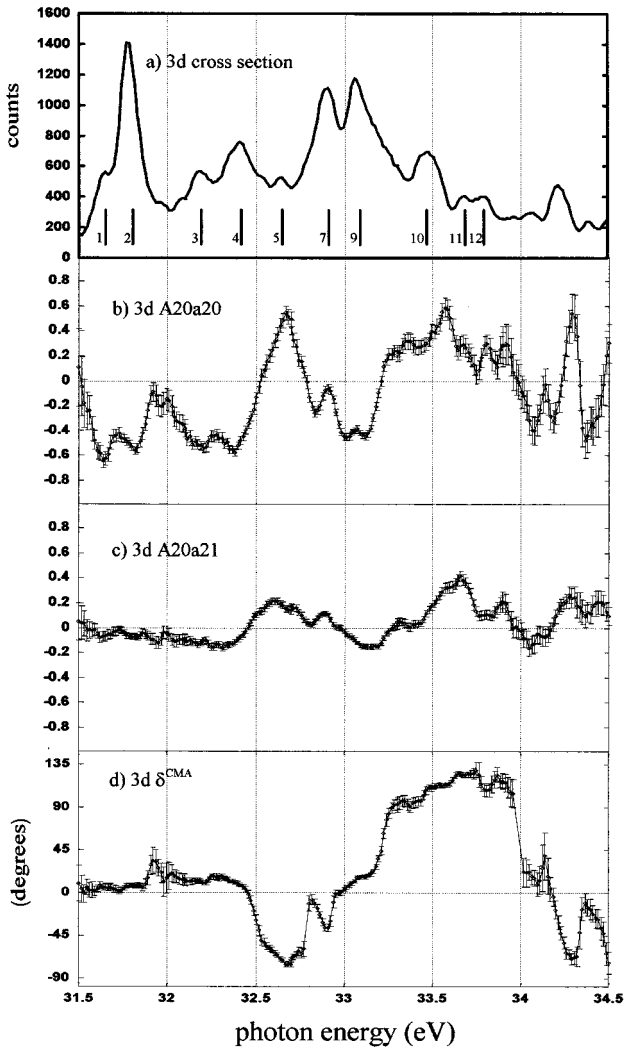

FIG. 9. The (a) cross section, parameters (b) $\overline{a_{20}}$ and (c) $\overline{a_{21}}$, and (d) phase tilt in the $3d$ channel measured by the CMA as a function of the photon energy. The marks in (a) represent the positions of the resonance features presented in Table III.

section one can find β in the $4s$ channel in the region of the $J=2$ resonance by using results of the ES measurements. The phase tilt (25) for the channels with $J=2$ reduces to

$$\tan 2\,\delta^{\mathrm{ES}}(\theta)=-\frac{6f(X)\sin 2\theta+15\,\sin 4\theta}{f(X)(1+6\,\cos 2\theta)+15\,\cos 4\theta}, \quad (32)$$

where $f(X)$ is defined by Eq. (29). Figure 10 shows the experimental results of the phase tilt $\delta^{\mathrm{ES}}(\theta)$ taken at the photon energy of 33.0 eV for decay in the $4s$ channel. These data are extracted from the η dependence of the ES signal at different spectrometer angles θ. Measurements are in fair agreement with the theoretical prediction of a ${}^1D_2$ resonance for pure LS coupling,

$$\tan 2\,\delta^{\mathrm{ES}}(\theta)=-\frac{6\,\sin 2\theta+9\,\sin 4\theta}{1+6\,\cos 2\theta+9\cos\,4\theta}, \quad (33)$$

whereas a ${}^3D_1$ resonance would result in the linear relation of $\delta^{\mathrm{ES}}(\theta)=-2\theta$. The best fit of Eq. (32) to the data using Eq. (31) gives $\beta=0.87(3)$ in excellent agreement with the

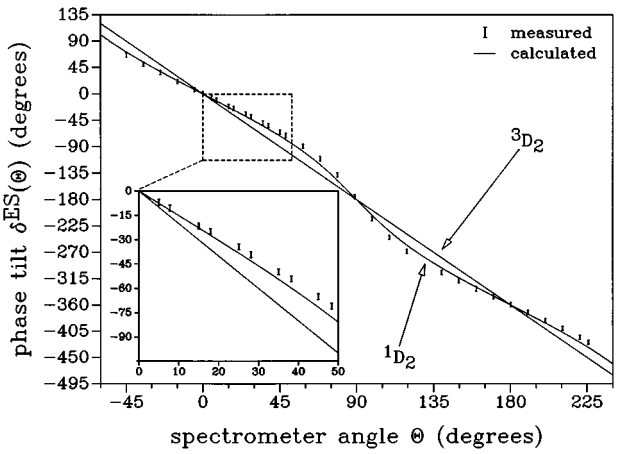

FIG. 10. Phase tilt $\delta^{ES}(\theta)$ in the $4s$ channel measured at a photon energy of 33.0 eV as a function of the ES position. The solid curves are the theoretical predictions for $^1D_2$ and $^3D_2$ ionization channels.

value from the CMA measurements (Sec. IV A). This shows the violation of the LS coupling and points to a consistency of the ES and CMA measurements. The question of the consistency is very important for the combined ES plus CMA analysis and is considered in more detail in the next subsection.

The generalized anisotropy parameters measured in the case of ionization with fixed J do not give independent information. Indeed one can obtain from Eqs. (2)–(4), taking $J_0=1$,

$$\beta_{202}=3(-1)^J\left(\frac{3}{5}\right)^{1/2}\begin{Bmatrix}1 & 1 & J\\ 1 & 1 & 2\end{Bmatrix}, \tag{34}$$

$$\beta_{220}=\beta_{022}=-\left(\frac{3}{10}\right)^{1/2}\beta, \tag{35}$$

$$\beta_{222}=(-1)^{J+1}\frac{3}{\sqrt{2}}\begin{Bmatrix}1 & 1 & J\\ 1 & 1 & J\\ 2 & 2 & 2\end{Bmatrix}\begin{Bmatrix}J & J & 2\\ 1 & 1 & 1\end{Bmatrix}^{-1}\beta. \tag{36}$$

Note that Eqs. (34)–(36) are valid for ionization into any ionic state provided J is fixed. In contrast, the formula

$$\beta_{242}=\frac{3\sqrt{6}}{5\sqrt{35}}(10\beta-7), \tag{37}$$

which follows from Eqs. (2)–(4) and (29)–(31), is valid only for the $4s$ channel (recall that only $J=2$ can contribute to the β_{242} due to the triangle rules). It follows that the present measurements are sufficient only for a determination of $f(X)$, Eq. (29), but not the complex parameter X, Eq. (30). Therefore it is impossible to find both the ratio of the real values of the reduced matrix elements $D_{3/2}$ and $D_{5/2}$ and the phase shift difference $\delta_{3/2}-\delta_{5/2}$ for ionization into the $\varepsilon d_{3/2}$ and $\varepsilon d_{5/2}$ continua. Using $\beta=0.87(3)$ one obtains from Eqs. (29) and (31) the equation

$$(\mathrm{Re}X-\mu)^2+(\mathrm{Im}X)^2=R^2, \tag{38}$$

which determines a circle of allowed values in the X plane with the position of the center and the radius given by $\mu=1.4^{-0.2}_{+0.4}$ and $R=1.3\pm0.3$. Note that our case of fixed $J=2$ differs from those when both continua εd and εs contribute to the photoionization. In these cases the parameters $\cos(\delta_d-\delta_s)$ and D_s/D_d can be extracted neglecting relativistic interactions from the measurements with two linear polarized photon beams [34,35].

Figures 11 and 12 show (as an example in the energy range 32.7–33.3 eV for the decay channels $4s$ and $3d$) the cross sections, the anisotropy parameter β, and the other four generalized anisotropy parameters. The latter are extracted from the measurements by the use of Eqs. (9)–(13). For the parameters β_{220}, β_{202}, β_{222}, and β_{242} only their products with the initial alignment A_{20} can be determined. Substituting $J=2$ and $\beta=0.87(3)$ into Eqs. (34)–(37) one obtains $\beta_{202}=0.077$, $\beta_{220}=-0.48(2)$, $\beta_{222}=0.081(2)$, and $\beta_{242}=0.42(8)$. The solid line for β in Fig. 11(b) shows the value 0.87 extracted from independent ES and CMA measurements. Solid lines in Figs. 11(c)–11(f) mark the values of $A_{20}\beta_{k_0kk_\gamma}$ assuming the ''ideal'' initial alignment $A_{20}=-\sqrt{2}$. The predicted values show some deviations from

TABLE III. Tentative assignment of resonance structures observed.

Number of state	Energy (eV) with respect to the ground state	Energy (eV) with respect to the excited state	Assigned dominating angular momentum J	Observed decay channels
1	34.60	31.65	1	$3d$,$4p$
2	34.70	31.75	1	$3d$,$4p$
3	35.15	32.20	1	$3d$,$4p$
4	35.35	32.40	1	$3d$,$4p$
5	35.55	32.60	2	$4s$,$3d$,$4p$
6	35.80	32.85	2	$4s$
7	35.85	32.90	0	$3d$,$4p$
8	35.95	33.00	2	$4s$
9	36.00	33.05	1	$3d$,$4p$
10	36.40	33.45	2	$4s$,$3d$,$4p$
11	36.65	33.70	2	$4s$,$3d$
12	36.75	33.80	0	$4s$,$3d$

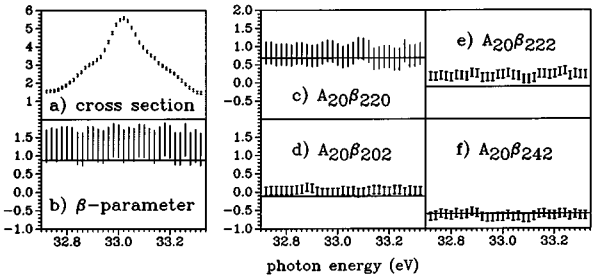

FIG. 11. Set of six parameters for photoionization from the excited and aligned $3p^6 4s4p\ ^1P_1$ state of calcium in the $4s$ channel: (a) the cross section (in arbitrary units), (b) the anisotropy parameter β, and the other four generalized anisotropy parameters (c) $A_{20}\beta_{220}$, (d) $A_{20}\beta_{202}$, (e) $A_{20}\beta_{222}$, and (f) $A_{20}\beta_{242}$ as functions of the photon energy. The solid lines represent the theoretical predictions.

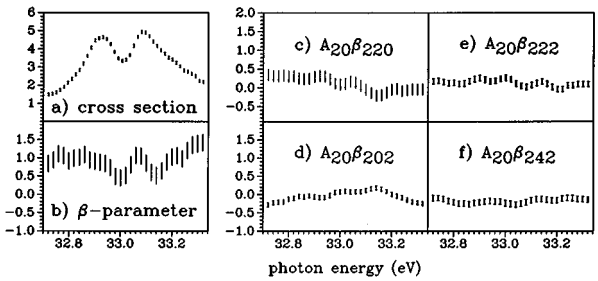

FIG. 12. Set of six parameters of photoionization from the excited and aligned $3p^6 4s4p\ ^1P_1$ state of calcium in the $3d$ channel: (a) the cross section (in arbitrary units), (b) the anisotropy parameter β, and the other four generalized anisotropy parameters (c) $A_{20}\beta_{220}$, (d) $A_{20}\beta_{202}$, (e) $A_{20}\beta_{222}$, and (f) $A_{20}\beta_{242}$ as functions of the photon energy.

the experiment. For example, they are not within the limits of experimental error for the small parameter $A_{20}\beta_{222}$. Nevertheless, in general there is reasonable agreement between the experiment and the predictions.

Note that as a result the electron spectroscopic data indicate almost ideal pumping ($A_{20}=-\sqrt{2}$) for the laser-excited intermediate state. Furthermore, nonzero values of the β_{242} [Figs. 11(f) and 12(f)] point to a contribution from channels with $J=2$ over the whole energy range shown. This is in accordance with the discussion of Sec. IV on the parameters $\overline{a_{21}}$ in the $4s$, $4p$, and $3d$ channels.

B. Consistency of the measurements

Due to the difficulties of the combined ES plus CMA measurements outlined in Sec. III A it is very important to check the mutual consistency of the two independent ES and CMA experiments. The apparent agreement found in the values of β in the $4s$ channel is not completely sufficient because it is based on measurements of the phase tilt only. This property is inherently stable against the value of the initial atomic alignment and against the difficulties encountered concerning the adjustment of the different beams with respect to each other. Therefore a more detailed discussion will be presented.

Assume now that the efficiency of the ES changes with the angle θ and also the effective alignment of the target is different for experiments with the CMA and ES, being A_{20}^{CMA} and A_{20}^{ES}, respectively. Repeating the derivation of Eqs. (7)–(13) it is easy to show that instead of Eq. (13) one must use

$$R_{\theta,\eta}=r(\theta)\frac{I(\theta,\eta)}{I(m,0^\circ)}\frac{(\alpha+2)W(0^\circ)+2(\alpha-1)W(90^\circ)}{W(0^\circ)+2W(90^\circ)}-1, \tag{39}$$

where $\alpha=A_{20}^{\mathrm{ES}}/A_{20}^{\mathrm{CMA}}$ and the unknown coefficient $r(\theta)$ accounts for change of the ES efficiency when rotating from m to θ $[r(m)=1]$. Also, in the formulas (9)–(12) the alignment A_{20} should be replaced by A_{20}^{ES}, while in the formulas of Sec. III B A_{20}^{CMA} should be used instead of A_{20}. Substituting Eqs. (9)–(12) in Eqs. (16) and (17) and using Eq. (39) one obtains

$$\overline{a_{20}}=\frac{1}{\alpha}R_{m,0}=\frac{1}{\alpha}\left[\frac{(\alpha+2)W(0^\circ)+2(\alpha-1)W(90^\circ)}{W(0^\circ)+2W(90^\circ)}-1\right], \tag{40}$$

$$\overline{a_{21}}=\frac{1}{\alpha\pi\sqrt{2}}(R_{m,m}-R_{m,-m})=\frac{1}{\alpha\pi\sqrt{2}}\frac{I(m,m)-I(m,-m)}{I(m,0)}\frac{(\alpha+2)W(0^\circ)+2(\alpha-1)W(90^\circ)}{W(0^\circ)+2W(90^\circ)}. \tag{41}$$

The right-hand sides of Eqs. (40) and (41) are functions of α but not of $r(\theta)$. Therefore a comparison of the parameters $\overline{a_{20}}$ and $\overline{a_{21}}$ obtained by the CMA alone and by the combined ES plus CMA setup leads to the determination of α. The best consistency was obtained by the assumption of the trivial value $\alpha=1$.

For another check we took the values of the generalized anisotropy parameters from the combined measurements [Eqs. (9)–(12) and (39)], calculated the phase tilt $\delta^{\mathrm{ES}}(\theta)$ according to Eq. (25), and compared the results with the phase tilt independently measured by the ES alone. Using this procedure one can check the value $r(0^\circ)$. Again best consistency is obtained for $r(0^\circ)=1$. Therefore the trivial values of α and $r(0^\circ)$ are used throughout the paper. However, these two quantities depend on the actual experimental conditions and in general differ from unity. In the present case unity resembles the best approximation to the experimental situation encountered.

VI. CONCLUSION

Photoionization of atomic calcium from the excited and aligned $4s4p\,^1P_1$ state has been investigated experimentally by applying the technique of simultaneous action of laser pumping and synchrotron radiation in combination with methods of angle-resolved and angle-integrated electron spectroscopy. The investigation covers the energy range of photons, 31.5–34.5 eV. Ionization channels corresponding to different states of the residual calcium ion were studied. It has been shown theoretically that the present setup is complete for investigation of the photoionization by linear polarized light of the aligned target with the total angular momentum $J_0=1$. This process is characterized by six independent parameters: the cross section and five generalized anisotropy parameters including the conventional anisotropy of the photoelectrons from an unpolarized target. All these parameters were determined experimentally in a limited energy range (32.7–33.3 eV).

The measured cross sections in different ion final-state channels show several autoionizing features which have not been observed hitherto. Measurements in different ionization channels with changing of the direction of the laser polarization allow us to assign tentatively the dominating total angular momentum of structures observed.

A table of even core-excited autoionizing features in calcium is presented together with the corresponding observed decay channels. To distinguish ionization channels with different total angular momenta J a new method is applied which consists of measurements of the two independent parameters $\overline{a_{20}}$ and $\overline{a_{21}}$, in addition to the cross section in an angle-integrating mode. The new parameters are sensitive to the value of J and to the redistribution of ionization probabilities between channels with different J. They are helpful not only for identification of the resonances but also for revealing ionization thresholds which are not clearly seen in the cross sections.

It is found that ionization of the $4s$ electron leaving the ion in the excited $4p$ state ($4p$ channel) is the favorable mechanism to produce the single-charged calcium ions by the photoabsorption in the excited $4s4p\,^1P_1$ state in the range 31.5–34.5 eV. Ionization of the excited $4p$ electron leaving the calcium ion in the $4s$ ground state ($4s$ channel) is dominated by the $J=2$ channel and is less probable except at the peak at 33.0 eV photon energy. The photoelectron satellites are, in general, as strong as in the case of the photoionization from the ground state.

Using the phase tilt method we measure the anisotropy of photoelectrons in the $4s$ channel and find a violation of the LS-coupling scheme for the photoionization into this channel. By combining results of measurements with the angle-resolved rotatable electron spectrometer and angle-integrating cylindrical mirror analyzer a set of generalized anisotropy parameters in the channels $4s$ and $3d$ are obtained, including the conventional β parameter. This demonstrates the feasibility of such measurements by using crossed laser and synchrotron radiation beams.

ACKNOWLEDGMENTS

The authors gratefully acknowledge continuous support by the BMBF and the BESSY staff. A. N. G.-G. gratefully acknowledges the hospitality and financial support by the Technical University Berlin and financial support by the Deutsche Forschungsgemeinschaft.

[1] J. M. Bizau, F. Wuilleumier, P. Dhez, D. L. Ederer, J. L. Picqué, J. L. LeGouët, and P. Koch, in *Laser Techniques for Extreme Ultraviolet Spectroscopy*, edited by T. J. McIlrath and R. J. Freeman, AIP Conf. Proc. No. 90 (AIP, New York, 1982), p. 331.

[2] J. M. Bizau, F. Wuilleumier, D. L. Ederer, J. C. Keller, J. L. LeGouët, J. L. Picqué, B. Carre, and P. M. Koch, Phys. Rev. Lett. **55**, 1281 (1985).

[3] A. Nunnemann, Th. Prescher, M. Richter, M. Schmidt, B. Sonntag, H.-E. Wetzel, and P. Zimmermann, J. Phys. B **18**, L337 (1985).

[4] F. J. Wuilleumier, D. L. Ederer, and J. L. Picqué, Adv. At. Mol. Phys. **23**, 197 (1988).

[5] M. Meyer, B. Müller, A. Nunnemann, T. Prescher, E. von Raven, M. Richter, M. Schmidt, B. Sonntag, and P. Zimmermann, Phys. Rev. Lett. **59**, 2963 (1987).

[6] M. Pahler, C. Lorenz, E. v. Raven, J. Rüder, B. Sonntag, S. Baier, B. R. Müller, M. Schulze, H. Staiger, P. Zimmermann, and N. M. Kabachnik, Phys. Rev. Lett. **68**, 2285 (1992).

[7] B. Sonntag, and M. Pahler, in *New Directions in Research with Third-Generation Soft X-Ray Synchrotron Radiation Sources*, edited by A. S. Schlachter and F. J. Wuilleumier (Kluwer Academic, Dordrecht, 1994), p. 103.

[8] S. Baier, M. Schulze, H. Staiger, P. Zimmermann, C. Lorenz, J. Rüeder, M. Pahler, and B. Sonntag, J. Phys. B **27**, 1341 (1994).

[9] S. Baier, M. Schulze, H. Staiger, M. Wedowski, P. Zimmermann, C. Lorenz, J. Rüder, M. Pahler, and B. Sonntag, J. Phys. B **28**, L81 (1995).

[10] M. W. D. Mansfield and G. H. Newsom, Proc. R. Soc. London, Ser. A **357**, 77 (1977).

[11] J. M. Bizau, P. Gerard, F. J. Wuilleumier, and G. Wendin, Phys. Rev. A **36**, 1220 (1987); Phys. Rev. Lett. **53**, 2083 (1984).

[12] Y. Sato, T. Hoyaishi, Y. Itikawa, Y. Itoh, J. Murakami, T. Nagata, T. Sasaki, B. Sonntag, and A. Yagashita, J. Phys. B **18**, 225 (1985).

[13] D. M. P. Holland and K. Codling, J. Phys. B **14**, 2345 (1981).

[14] K. Ueda, J. B. West, K. J. Ross, H. Hamdy, H. J. Beyer, and H. Kleinpoppen, Phys. Rev. A **48**, R863 (1993).

[15] H. Hamdy, H.-J. Beyer, J. B. West, and H. Kleinpoppen, J. Phys. B **24**, 4957 (1991).

[16] H. J. Beyer, J. B. West, K. J. Ross, K. Ueda, N. M. Kabachnik, H. Hamdy, and H. Kleinpoppen, J. Phys. B **28**, L47 (1995).

[17] B. F. Sonntag, C. L. Cromer, J. M. Bridges, T. J. McIlrath, and T. B. Lucatorto, in *Short Wavelength Coherent Radiation: Generation and Applications*, edited by D. T. Attwood and J. Bokor, AIP Conf. Proc. No. 147 (AIP, New York, 1986), p. 412.

[18] M. Meyer, T. Prescher, E. von Raven, M. Richter, B. Sonntag, B. Müller, W. Fiedler, and P. Zimmermann, J. Phys. (Paris) Colloq. **48**, C9-547 (1987).
[19] S. Baier, W. Fiedler, B. R. Müller, M. Schulze, P. Zimmermann, M. Meyer, M. Pahler, Th. Prescher, E. von Raven, M. Richter, J. Rueder, and B. Sonntag, J. Phys. B **25**, 923 (1992).
[20] V. V. Balashov, A. N. Grum-Grzhimailo, and B. Zhadamba, Opt. Spektrosk. **65**, 529 (1988) [Opt. Spectrosc. USSR **65**, 315 (1988)].
[21] K. W. McLaughlin, D. S. Eschliman, O. P. Francis, and D. W. Duquette, Phys. Rev. A **49**, 240 (1994).
[22] M. Wedowski, K. Godehusen, F. Weisbarth, P. Zimmermann, Th. Dohrmann, A. von dem Borne, B. Sonntag, and A. N. Grum-Grzhimailo, J. Electron Spectrosc. Relat. Phenom. **75**, 61 (1995).
[23] N. A. Cherepkov, V. V. Kuznetsov, and A. A. Verbitskii, J. Phys. B **28**, 1221 (1995).
[24] S. Baier, A. N. Grum-Grzhimailo, and N. M. Kabachnik, J. Phys. B **27**, 3363 (1994).
[25] L.-W. He, C. E. Burkhardt, M. Ciocca, J. J. Leventhal, H.-L. Zhou, and S. T. Manson, Phys. Rev. A **51**, 2085 (1995).
[26] J. C. Hansen, J. A. Duncanson, Jr., R. Chien, and R. S. Berry, Phys. Rev. A **21**, 222 (1980).
[27] A. Siegel, J. Ganz, W. Bussert, and H. Hotop, J. Phys. B **16**, 2945 (1983).
[28] M. W. D. Mansfield and T. W. Ottley, Proc. R. Soc. London, Ser. A **365**, 413 (1979).
[29] C. E. Moore, *Atomic Energy Levels*, Natl. Bur. Stand. (U.S.) Circ. No. 467 (U. S. GPO, Washington, DC, 1949), Vol. I.
[30] V. Pejcev, T. W. Ottley, D. Rassi, and K. J. Ross, J. Phys. B **11**, 531 (1978).
[31] W. Schmitz, B. Breuckmann, and W. Mehlhorn, J. Phys. B **9**, L493 (1976).
[32] I. C. Lyon, B. Peart, K. Dolder, and J. B. West, J. Phys. B **20**, 1471 (1987).
[33] V. K. Ivanov and J. B. West, J. Phys. B **26**, 2099 (1993).
[34] O. C. Mullins, R. Chien, J. E. Hunter III, J. S. Keller, and R. S. Berry, Phys. Rev. A **31**, 321 (1985).
[35] C. Kerling, N. Böwering, and U. Heinzmann, J. Phys. B **23**, L629 (1990).
[36] J. B. West, K. Ueda, N. M. Kabachnik, K. Ross, H. J. Beyer, and H. Kleinpoppen, Phys. Rev. A **35**, R9 (1996).